

Article

Stability of Noncentrosymmetric Square Skyrmiон Crystals with Easy-Axis and Easy-Plane Magnetic Anisotropy

Satoru Hayami 

Graduate School of Science, Hokkaido University, Sapporo 060-0810, Japan; hayami@phys.sci.hokudai.ac.jp

Abstract: We investigate the stability tendency of a magnetic skyrmion crystal in noncentrosymmetric tetragonal systems with the Dzyaloshinskii–Moriya interaction. We show that the stability region of the square skyrmion crystal on a square lattice depends on the Ising-type magnetic anisotropic interaction by performing the simulated annealing for the spin model. The easy-axis anisotropic interaction tends to narrow the region where the square skyrmion crystal is stabilized when the magnetic field is applied in the out-of-plane direction. In contrast, the easy-plane anisotropic interaction tends to enlarge the stability region. Meanwhile, the square skyrmion crystal induced by the easy-axis anisotropic interaction is robust compared with that induced by the easy-plane anisotropic interaction when the magnetic field is tilted from the out-of-plane to the in-plane direction. The results indicate that the instability toward the square skyrmion crystal in noncentrosymmetric crystals is sensitive to both magnetic anisotropy and magnetic fields.

Keywords: skyrmion crystal; Dzyaloshinskii–Moriya interaction; magnetic field; square lattice; magnetic anisotropy

1. Introduction



Citation: Hayami, S. Stability of Noncentrosymmetric Square Skyrmiон Crystals with Easy-Axis and Easy-Plane Magnetic Anisotropy. *Magnetism* **2024**, *4*, 368–382. <https://doi.org/10.3390/magnetism4040024>

Academic Editor: Kai Wang

Received: 28 August 2024

Revised: 19 October 2024

Accepted: 21 October 2024

Published: 2 November 2024



Copyright: © 2024 by the author. Licensee MDPI, Basel, Switzerland. This article is an open access article distributed under the terms and conditions of the Creative Commons Attribution (CC BY) license (<https://creativecommons.org/licenses/by/4.0/>).

Spatial inversion symmetry is significant in determining physical properties in materials [1]. The lack of the inversion center in crystals often leads to fascinating entanglement between spin and momentum, which results in antisymmetric spin splitting in the electronic band structure depending on the crystal symmetry [2–5], such as Rashba-type spin splitting under polar symmetry [6–9], Weyl-type spin splitting under chiral symmetry [10,11], and Ising-type spin splitting under trigonal symmetry [12–16]. Such a spin-momentum coupling becomes a source of various physical phenomena, including the spin Hall effect [17–21], the Edelstein effect [22–28], the nonreciprocal transport [29–39], and the magnetoelectric effect [40–50]. In this way, the system without spatial inversion symmetry provides a rich playground for new functionalities that might be utilized for future electronic device applications.

The absence of spatial inversion symmetry also affects the stability of magnetic states. The most typical example is the Dzyaloshinskii–Moriya (DM) interaction [51,52], which originates from the relativistic spin–orbit coupling. Since the DM interaction tends to tilt the neighboring spin moments in a noncollinear way, the competition between the DM interaction and the ferromagnetic exchange interaction leads to a spiral state at zero field and a magnetic skyrmion crystal (SkX) in an external magnetic field [53–61], where the SkX corresponds to a triple-Q state as a consequence of a superposition of three spiral waves; each skyrmion, which is regarded as a topologically nontrivial particle [62,63], forms a triangular lattice. Reflecting topologically nontrivial spin textures in the SkX, various physical properties have been additionally revealed, such as the topological Hall/Nernst effect [64–72], current-induced motions [73–80], and nucleation by current and electric field pulses [81–87]. Thus, investigating the stability of the SkX based on the microscopic magnetic interactions is important. Especially, it is desired to understand the robustness of the SkX against magnetic anisotropy, which is sometimes neglected, distinct from the DM

interaction. For that purpose, the effect of magnetic anisotropy on the stability of the SkX has been studied for different spin models for years [88–92].

In the present study, we examine the ground-state stability tendency of the double-Q SkX rather than the triple-Q SkX in noncentrosymmetric tetragonal magnets against magnetic anisotropy, where the double-Q SkX consists of a superposition of two spiral waves, and is characterized by the square alignment of the skyrmions owing to lattice anisotropy. Compared with the triple-Q SkX, the stability of the double-Q SkX has not been fully elucidated [93,94]. Meanwhile, the square SkX has been recently found in both noncentrosymmetric magnets, like $\text{Co}_{10-x/2}\text{Zn}_{10-x/2}\text{Mn}_x$ [95–99] and Cu_2OSeO_3 [100,101], and centrosymmetric magnets, like GdRu_2Si_2 [102–106] and GdRu_2Ge_2 [107]. Motivated by such a situation, we numerically study the stability of the square SkX by focusing on the role of the easy-axis and easy-plane magnetic anisotropic interactions in frustrated tetragonal magnets with competing exchange interactions leading to a finite- q ordering. Through the simulated annealing for the classical spin model with the DM interaction and easy-axis or easy-plane anisotropic interaction, we investigate the stability of the square SkX for two situations: One is the stability tendency in terms of the magnitude of the out-of-plane magnetic field and the other is the stability tendency in terms of the magnetic field rotation. For the former case, we show that the easy-axis anisotropic interaction tends to destabilize the SkX, while the easy-plane anisotropic interaction tends to stabilize the SkX. For the latter case, we show that the SkX with the easy-axis anisotropic interaction tends to be robust against the field rotation, while that with the easy-plane anisotropic interaction is sensitive to the field direction.

The remainder of this paper is structured as follows. First, we introduce the spin model and numerical method based on simulated annealing in Section 2. Then, we show the effect of the easy-axis and easy-plane anisotropic interactions on the stabilization of the square SkX in the out-of-plane magnetic field in Section 3. We also discuss the stability tendency under magnetic field rotation. Section 4 is devoted to a conclusion of the present paper.

2. Model and Method

In order to investigate the stability of the square SkX, we consider the spin model on a two-dimensional square lattice under polar C_{4v} symmetry; we set the lattice constant as unity. The effective spin model is given by [108]

$$\mathcal{H} = -2 \sum_{\nu} \left[JS_{Q_{\nu}} \cdot S_{-Q_{\nu}} + I^z S_{Q_{\nu}}^z S_{-Q_{\nu}}^z + i D_{Q_{\nu}} \cdot (S_{Q_{\nu}} \times S_{-Q_{\nu}}) \right] - \sqrt{NB} \cdot S_0, \quad (1)$$

where $S_{Q_{\nu}} = (S_{Q_{\nu}}^x, S_{Q_{\nu}}^y, S_{Q_{\nu}}^z)$ represents the Q_{ν} component of the spin, which is related to the Fourier transform of the classical localized spin $S_i = (S_i^x, S_i^y, S_i^z)$ with a fixed spin length $|S_i| = 1$. The first term represents the momentum-resolved Heisenberg exchange interaction with the coupling constant J . We here simplify the interaction by considering the contribution from a few ordering wave vectors for $\nu = 1, 2$: $Q_1 = (2\pi/5, 0)$ and $Q_2 = (0, 2\pi/5)$, which are related by fourfold rotational symmetry, as shown in the right panel of Figure 1; the prefactor 2 means the contribution from $-Q_1$ and $-Q_2$. It is noted that the magnitude of the interactions at Q_1 and Q_2 is the same owing to the fourfold rotational symmetry of the square lattice. We ignore the interactions at the other wave vectors in the Brillouin zone; such a simplification is justified when the ground-state spin configuration is characterized by a linear combination of the spin density waves at Q_1 and/or Q_2 [109]. The microscopic origin of this interaction is the frustrated short-range exchange interaction or the long-range Ruderman–Kittel–Kasuya–Yosida interaction, the latter of which is dictated by the nesting of the Fermi surface [110–112].

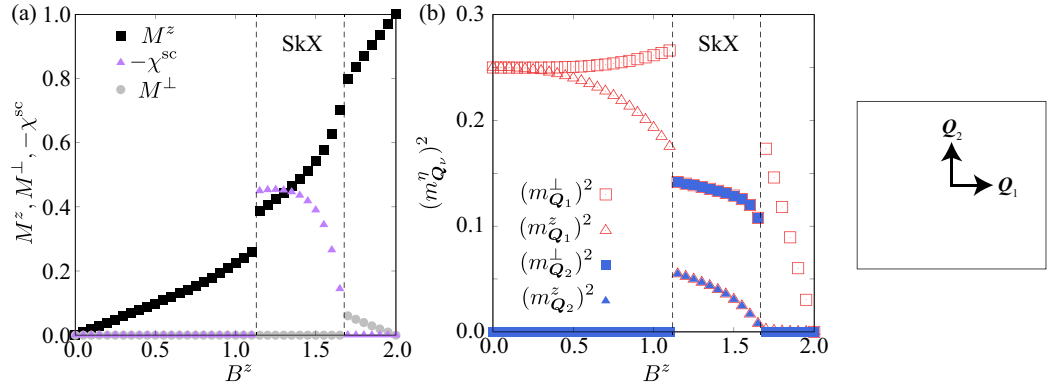


Figure 1. B^z dependence of (a) the in-plane magnetization, M^\perp , the out-of-plane magnetization, M^z , and the scalar spin chirality, χ^{sc} , and (b) the squared momentum-resolved magnetic moments $(m_{Q_\nu}^\eta)^2$ for $\eta = \perp, z$ and $\nu = 1, 2$ in the absence of the Ising-type magnetic anisotropy $I^z = 0$ for $B^x = 0$. The vertical dashed lines represent the phase boundaries between the SkXs and other topologically trivial magnetic phases. In the right panel, the ordering wave vectors Q_1 and Q_2 in the first Brillouin zone are schematically shown.

The second and third terms in the model in Equation (1) denote the magnetic anisotropic interactions, which arise from the relativistic spin–orbit coupling. The second term stands for the easy-axis-type anisotropic interaction with the coupling constant I^z ; $I^z > 0$ ($I^z < 0$) corresponds to the easy-axis (easy-plane) interaction. Meanwhile, the third term stands for the DM interaction brought about by the noncentrosymmetric lattice structure [113]; the appearance of the imaginary number in the coefficient is due to the momentum-space representation of the DM interaction. From the polar C_{4v} symmetry, the nonzero component of the DM vector, $D_{Q_\nu}^y$, is given by $D_{Q_1}^y = -D_{Q_2}^x \equiv D$; other components are zero. The sign of the DM interaction determines the helicity of the single- Q spiral state and double- Q SkX, whose difference does not affect the following phase diagrams. Although we suppose that the DM interaction originates from noncentrosymmetric lattice structures under the C_{4v} symmetry in bulk, it is possible to take into account the effect of the interfacial DM interaction when the interface structure is considered. In addition, we ignore the effect of other symmetry-allowed magnetic anisotropic interactions, such as the bond-dependent anisotropic interaction, for simplicity [114]. The fourth term in Equation (1) represents the Zeeman coupling in momentum space to take into account the effect of the external magnetic field in the zx plane, i.e., $\mathbf{B} = (B^x, 0, B^z)$; the g -factor is renormalized into B . S_0 represents the $\mathbf{q} = \mathbf{0}$ component of spins and N is the total number of spins. In the following calculations, we set $J = 1$ and $D = 0.3$, and investigate the stability of the square SkX while changing B^x and B^z for several I^z .

For the spin model in Equation (1), we construct the magnetic phase diagram at a low temperature, $T/J = 10^{-4}$, in the bulk system by performing the simulated annealing in the following procedure. We start from a random spin configuration at a high temperature, $T_0 = 1.5$, which is taken so as to be larger than J . Then, we gradually reduce the temperature with a ratio of $T_{n+1} = 0.999999T_n$ (T_n is the n th-step temperature) in each Monte Carlo sweep. At each temperature, we locally update all the spins in real space for variables θ and ϕ for $S_i = (\cos \phi \sin \theta, \sin \phi \sin \theta, \cos \theta)$ based on the standard Metropolis algorithm. We repeat the above procedure until the temperature reaches the final temperature, $T = 10^{-4}$. At the final temperature, we perform 10^5 – 10^6 further Monte Carlo sweeps for measurements. We confirm that the final state is not affected by the initial spin configuration. We show the results for the system size with the total number of spins $N = 10^2$ under the periodic boundary conditions, although we confirm that the qualitative results are not altered for $N = 20^2$.

The magnetic phases obtained by the simulated annealing are identified by the spin structure factor and the scalar spin chirality. The spin structure factor, which gives the measure of the correlation between spins, is given by

$$S_s^{\eta\eta}(\mathbf{q}) = \frac{1}{N} \sum_{i,j} S_i^\eta S_j^\eta e^{i\mathbf{q}\cdot(\mathbf{r}_i-\mathbf{r}_j)}, \quad (2)$$

for the spin component $\eta = x, y, z$. Here, \mathbf{r}_i is the position vector at site i and \mathbf{q} is the wave vector in the first Brillouin zone. The \mathbf{Q}_v component of the magnetic moments is calculated by using $S_s^{\eta\eta}(\mathbf{q})$ as

$$m_{\mathbf{Q}_v}^\eta = \sqrt{\frac{S_s^{\eta\eta}(\mathbf{Q}_v)}{N}}. \quad (3)$$

We set the in-plane component of $m_{\mathbf{Q}_v}^\eta$ as $(m_{\mathbf{Q}_v}^\perp)^2 = (m_{\mathbf{Q}_v}^x)^2 + (m_{\mathbf{Q}_v}^y)^2$. The uniform magnetization is calculated by

$$M^\eta = \frac{1}{N} \sum_i S_i^\eta, \quad (4)$$

for $\eta = x, y, z$. We also calculate the in-plane magnetization as $M^\perp = \sqrt{(M^x)^2 + (M^y)^2}$.

Meanwhile, we calculate the scalar spin chirality by

$$\chi^{sc} = \frac{1}{2N} \sum_i \sum_{\delta,\delta'=\pm 1} \delta \delta' \mathbf{S}_i \cdot (\mathbf{S}_{i+\delta\hat{x}} \times \mathbf{S}_{i+\delta'\hat{y}}), \quad (5)$$

where \hat{x} (\hat{y}) represents a shift by the lattice constant of the square lattice in the x (y) direction. Nonzero χ^{sc} implies the emergence of the SkX (or topological spin textures) [115], where the skyrmion number under discrete lattice structures is calculated in the manner of Ref. [116].

3. Results

We discuss the stability of the square SkX against Ising-type magnetic anisotropy by considering the two situations. One is the case with the magnetic field along the out-of-plane direction in Section 3.1, and the other is the case with the magnetic field in the zx plane in Section 3.2.

3.1. In an Out-Of-Plane Magnetic Field

In this section, we consider the situation where the magnetic field is applied along the out-of-plane direction, i.e., $B^x = 0$ and $B^z \neq 0$. Figure 1a shows the B^z dependence of the in-plane and out-of-plane magnetizations, M^\perp and M^z , and the scalar spin chirality, χ^{sc} , at $D = 0.3$ in the absence of the Ising-type anisotropic interaction ($I^z = 0$). At zero field, the single- Q cycloidal spiral state is stabilized, where the spiral plane lies on the zx (yz) plane for the ordering wave vector \mathbf{Q}_1 (\mathbf{Q}_2). The stabilization of such a single- Q cycloidal state is attributed to the interplay between the Heisenberg-type exchange interaction and the DM interaction. Since there is no preferable spin direction in the single- Q spiral state, the spiral plane becomes circular, which results in the equal intensity of $(m_{\mathbf{Q}_1}^\perp)^2$ and $(m_{\mathbf{Q}_1}^z)^2$, as shown in Figure 1b. Owing to the coplanar spin configuration, there is no scalar spin chirality.

When the z -directional magnetic field is applied, the magnetization M^z is linearly induced, as shown in Figure 1a. The introduction of the magnetic field changes the spiral plane from a circular shape to an elliptical shape, as found in the relationship of $(m_{\mathbf{Q}_1}^\perp)^2 \neq (m_{\mathbf{Q}_1}^z)^2$ in Figure 1b; $(m_{\mathbf{Q}_1}^\perp)^2$ tends to be larger than $(m_{\mathbf{Q}_1}^z)^2$ due to the spin-flop tendency against the magnetic field direction; the perpendicular spin component to the magnetic field is enhanced, while the parallel spin component is suppressed. We show the real-space spin configuration of the single- Q state at $B^z = 0.7$ in Figure 2a, where the region with the positive z -spin component is wider than that with the negative z -spin component.

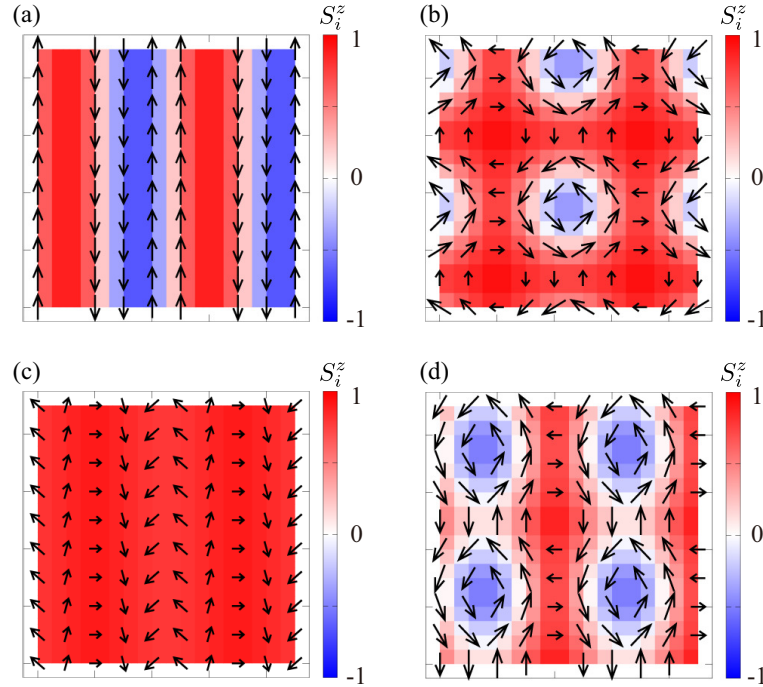


Figure 2. Real-space spin configurations of (a) the single- Q spiral state at $I^z = 0$ and $B^z = 0.7$, (b) the SkX at $I^z = 0$ and $B^z = 1.4$, (c) the single- Q spiral state at $I^z = 0$ and $B^z = 1.75$, and (d) the SkX at $I^z = -0.4$ and $B^z = 0.65$ for $B^x = 0$. The arrows show the direction of the spin moments and the colors show the z -spin component. The spin configurations are obtained by the simulated annealing.

With the increase in B^z , the single- Q state turns into the square SkX with a jump of M^z , as shown in Figure 1a; their transition is characterized by a first-order phase transition. The spin configuration of the square SkX consists of a superposition of the double- Q spin density waves at Q_1 and Q_2 . As shown in Figure 1b, the magnitudes of both xy and z components in magnetic moments are equal for the Q_1 and Q_2 components, i.e., $(m_{Q_1}^\perp)^2 = (m_{Q_2}^\perp)^2$ and $(m_{Q_1}^z)^2 = (m_{Q_2}^z)^2$. The SkX spin texture is found in the real space, as shown in Figure 2b; the skyrmion core denoted as $S_i^z = -1$ periodically aligns in a square-lattice way, which is located at the center of the square plaquette rather than the lattice site [117]. According to the noncoplanar spin configuration, the scalar spin chirality becomes nonzero [Figure 1a]. Since the winding number around the skyrmion core is $+1$, the skyrmion number defined by the product of the z -spin polarization and the vorticity is given by -1 [59]. It is noted that the vortices with the opposite winding number appear between the skyrmion cores.

With further increasing B^z , the SkX turns into the single- Q state again; the magnetization and the scalar spin chirality show discontinuous changes, as shown in Figure 1a. This single- Q spin configuration shows a nonzero transverse magnetization, $M^\perp \neq 0$, which indicates that the spiral plane is tilted from the zx (or yz) plane to the xy plane in order to gain energy by the Zeeman coupling; the real-space spin configuration is shown in Figure 2c. Although the high-field single- Q state is characterized by the noncoplanar spin configuration, the uniform scalar spin chirality becomes zero. The single- Q state finally changes into the fully polarized state at $B^z = 2$.

Next, we consider the effect of I^z on the stability region of the square SkX. We show the case for the easy-axis anisotropic interaction; the result for $I^z = 0.2$ is shown in Figure 3a,b and the result for $I^z = 0.4$ is shown in Figure 3c,d. Compared with the result for $I^z = 0$ in Figure 1a,b, the phase sequences against B^z for $I^z > 0$ are qualitatively similar to each other.

Meanwhile, one finds that the region of the square SkX for $I^z = 0.2$ becomes narrower than that for $I^z = 0$. Such a feature is also found for $I^z = 0.4$ in Figure 3c,d. Thus, the easy-axis anisotropic interaction tends to make the square SkX unstable, which is opposite to the SkX in centrosymmetric magnets; the SkX is more stabilized when the easy-axis anisotropic

interaction increases [118,119]. We also find that the easy-axis anisotropic interaction makes the high-field single-Q state unstable. This is because the easy-axis anisotropic interaction favors the cycloidal spiral state on the zx (or yz) plane rather than the conical spiral state on the xy plane.

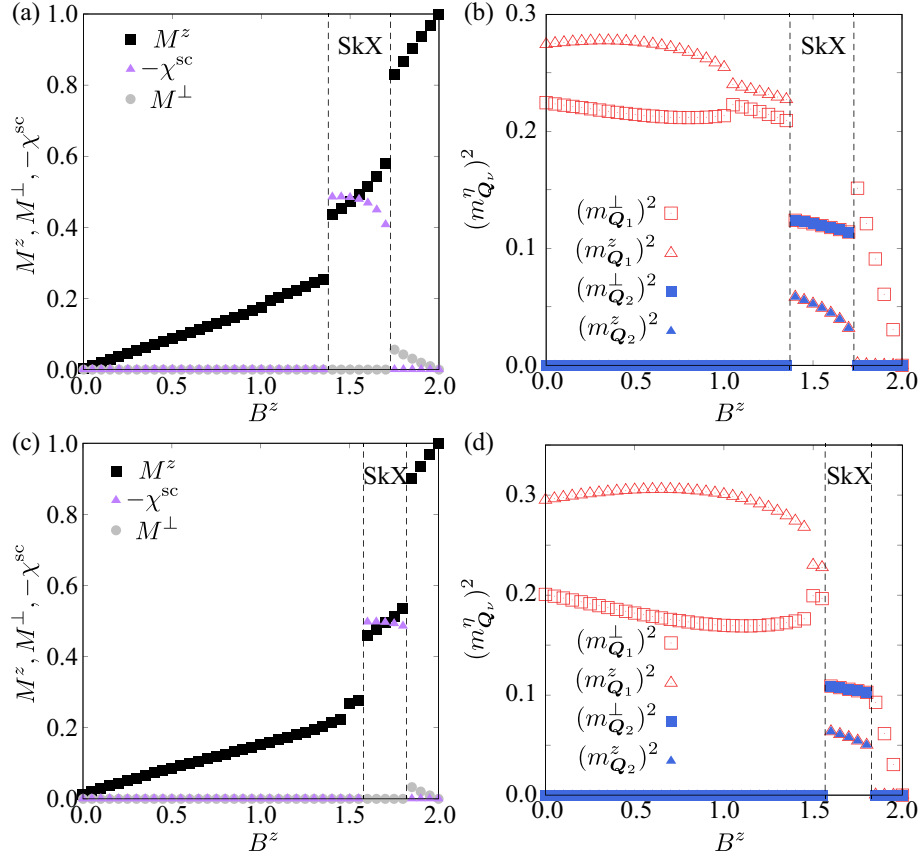


Figure 3. B^z dependence of (a,c) the in-plane magnetization, M^\perp , the out-of-plane magnetization, M^z , and the scalar spin chirality, χ^{sc} , and (b,d) the squared momentum-resolved magnetic moments $(m_{Q_\nu}^\eta)^2$ for $\eta = \perp, z$ and $\nu = 1, 2$ at (a,c) $I^z = 0.2$ and (b,d) $I^z = 0.4$ for $B^x = 0$. The vertical dashed lines represent the phase boundaries between different magnetic phases.

On the other hand, the easy-plane anisotropic interaction $I^z < 0$ leads to an opposite tendency to the easy-axis interaction $I^z > 0$. As shown in the cases of $I^z = -0.2$ in Figure 4a,b and $I^z = -0.4$ in Figure 4c,d, the regions of both the square SkX and the high-field single-Q state become wider. Since the easy-plane anisotropic interaction tends to favor the conical spiral state instead of the cycloidal spiral state, the spiral plane in the low-field single-Q state is also tilted from the zx (or yz) plane to the xy plane. Accordingly, the low-field single-Q state also accompanies the in-plane magnetization, M^\perp , as shown in Figure 4c. It is noted that the size of the skyrmion is not changed for both positive and negative I^z , since the periodicity of the skyrmion is characterized by the momentum-resolved interactions at Q_1 and Q_2 .

Moreover, we find a rectangular SkX at $B^z = 0.65$ and $I^z = -0.4$. In contrast to the square SkX, this state is characterized by the anisotropic double-Q spin modulations at Q_1 and Q_2 . In other words, $(m_{Q_1}^\perp)^2$ and $(m_{Q_1}^z)^2$ are not equal to $(m_{Q_2}^\perp)^2$ and $(m_{Q_2}^z)^2$, respectively. Reflecting such an anisotropic double-Q structure, the skyrmion core is elongated along the y direction so that the fourfold rotational symmetry is broken, as shown by the real-space spin configuration in Figure 2d. A similar rectangular SkX has also been found in centrosymmetric magnets with easy-axis single-ion anisotropy [94]. Thus, the present result indicates that the rectangular SkX can emerge in the noncentrosymmetric

magnets when the easy-plane anisotropic interaction is relatively large, although the stability region is much narrower compared with the square SkX.

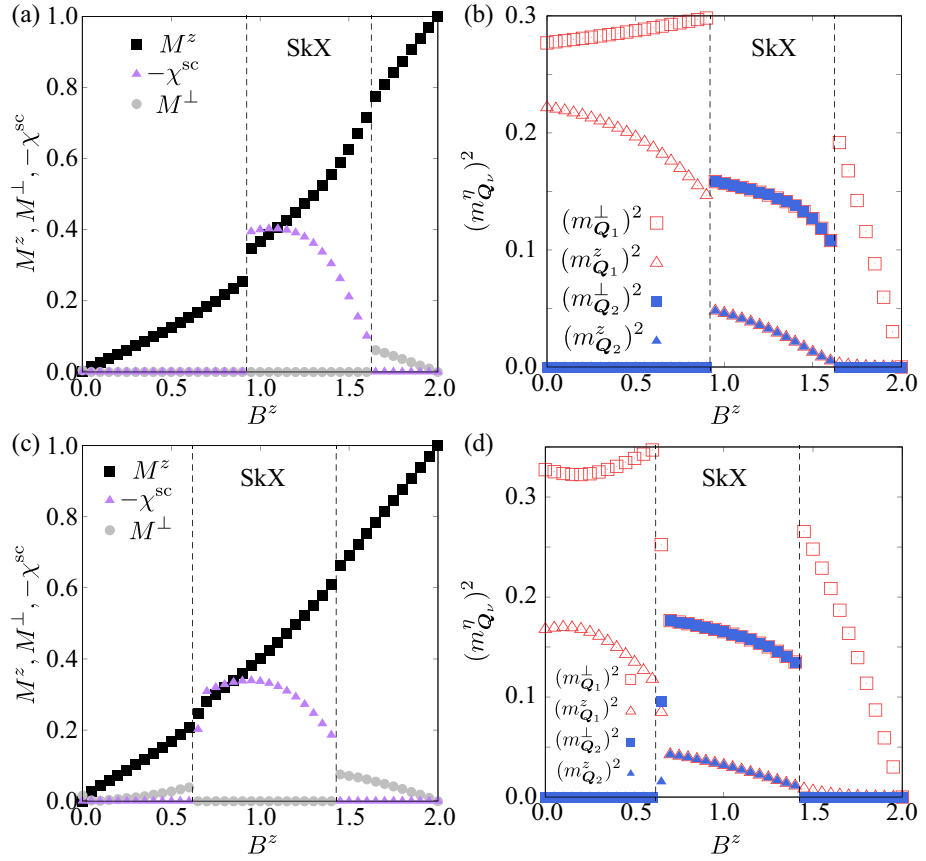


Figure 4. B^z dependence of (a,c) the in-plane magnetization, M^\perp , the out-of-plane magnetization, M^z , and the scalar spin chirality, χ^{sc} , and (b,d) the squared momentum-resolved magnetic moments $(m_{Q_\nu}^\eta)^2$ for $\eta = \perp, z$ and $\nu = 1, 2$ at (a,c) $I^z = -0.2$ and (b,d) $I^z = -0.4$ for $B^x = 0$. The vertical dashed lines represent the phase boundaries between the SkXs and other topologically trivial magnetic phases.

3.2. In a Tilted Magnetic Field

In this section, we further examine the stability of the square SkX by rotating the magnetic field in the zx plane. In the absence of I^z , the phase diagram in the plane of B^x and B^z is shown in Figure 5a. The square SkX becomes unstable when the in-plane field B^x is introduced; no SkX is stabilized for $B^x \gtrsim 0.19$ and all the regions are occupied by the single-Q state. Thus, the stability of the square SkX induced by the DM interaction on the square lattice is sensitive to the magnetic field direction. This might be attributed to the fact that we suppose that the position of the ordering wave vectors is not changed against the magnetic field direction. Such a feature has been found in the noncentrosymmetric SkX-hosting material EuPtSi [120–126], where the appearance of the SkX largely depends on the magnetic field direction [123,125,127–129].

We show the B^x dependence of spin and chirality quantities at $B^z = 1.3$ in Figure 6a,b. In the SkX region, the scalar spin chirality and the squared magnetic moments are almost constant against B^x , as shown in Figure 6a and 6b, respectively. Reflecting such a feature, the real-space spin configuration of the SkX at $B^x = 0.1$ in Figure 7a is almost the same as that at $B^x = 0$ in Figure 2b. The SkX is replaced by the single-Q spiral state at $B^x \simeq 0.18$ with the jumps of M^z and M^\perp ; the spin configuration of the single-Q spiral state is shown in Figure 7b.

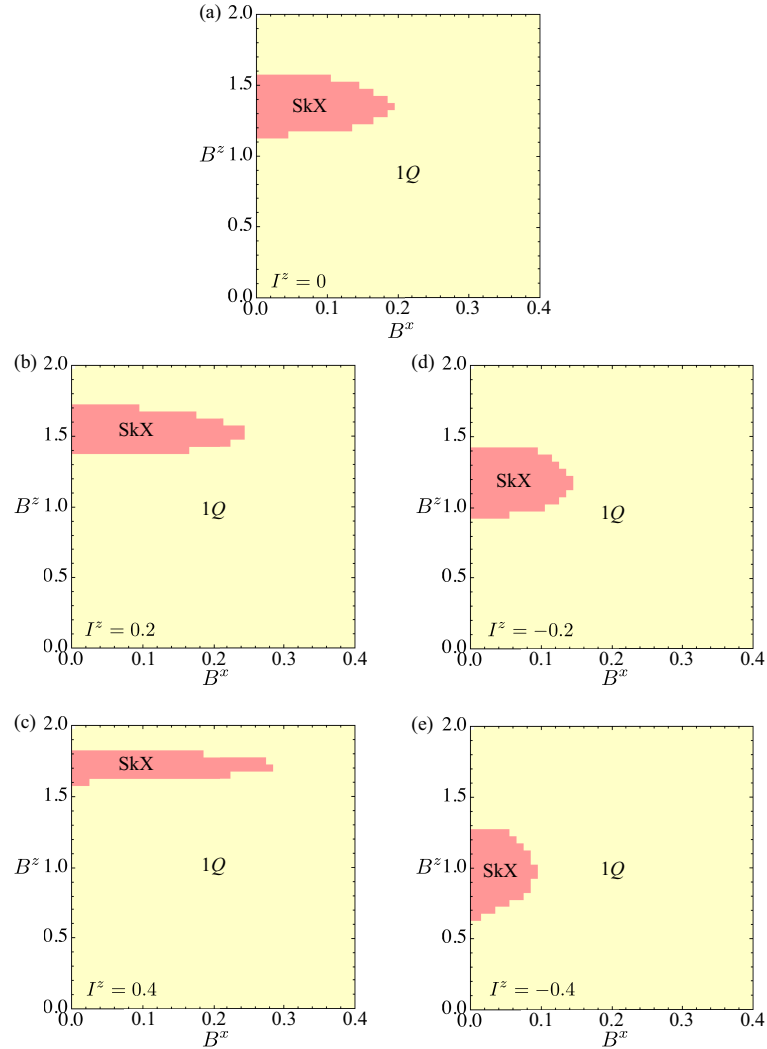


Figure 5. Mangetic phase diagrams in the tilted magnetic field on the zx plane at (a) $I^z = 0$, (b) $I^z = 0.2$, (c) $I^z = 0.4$, (d) $I^z = -0.2$, and (e) $I^z = -0.4$. 1Q and SkX stand for the single- Q and skyrmion crystal, respectively.

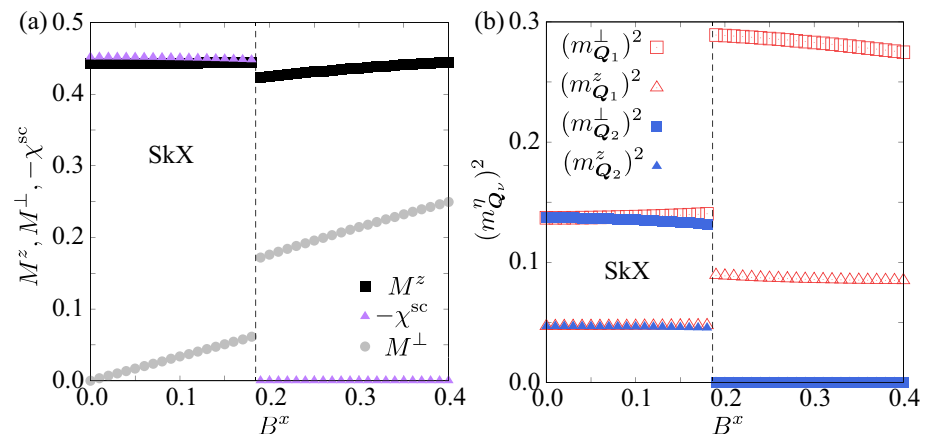


Figure 6. B^x dependence of (a) the in-plane magnetization, M^\perp , the out-of-plane magnetization, M^z , and the scalar spin chirality, χ^{sc} , and (b) the squared momentum-resolved magnetic moments $(m_{Q_\nu}^\eta)^2$ for $\eta = \perp, z$ and $\nu = 1, 2$ at $I^z = 0$ and $B^z = 1.3$. The vertical dashed lines represent the phase boundaries between the SkXs and other topologically trivial magnetic phases.

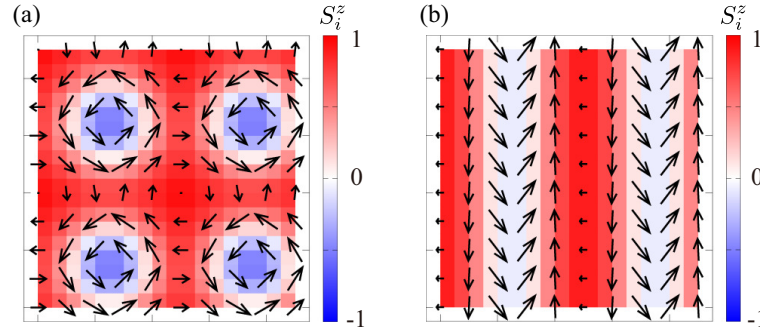


Figure 7. Real-space spin configurations of (a) the SkX at $I^z = 0$, $B^x = 0.1$, and $B^z = 1.3$ and (b) the single-Q spiral state at $I^z = 0$, $B^x = 0.2$, and $B^z = 1.3$. The arrows show the direction of the spin moments and the colors show the z-spin component. The spin configurations are obtained by the simulated annealing.

For the easy-axis anisotropic interaction $I^z > 0$, the phase diagrams are shown in Figure 5b for $I^z = 0.2$ and Figure 5c for $I^z = 0.4$. As shown in Section 3.1, the region of the square SkX against B^z becomes narrower when I^z becomes larger. Meanwhile, the square SkX is more robust against B^x for larger I^z . For example, the SkX is stable up to $B^x \simeq 0.24$ at $B^z = 1.5$ for $I^z = 0.2$, as shown in Figure 8a,b, and up to $B^x \simeq 0.28$ at $B^z = 1.7$ for $I^z = 0.4$, as shown in Figure 8c,d. In both cases, the SkX turns into the single-Q spiral state with a further increase in B^x .

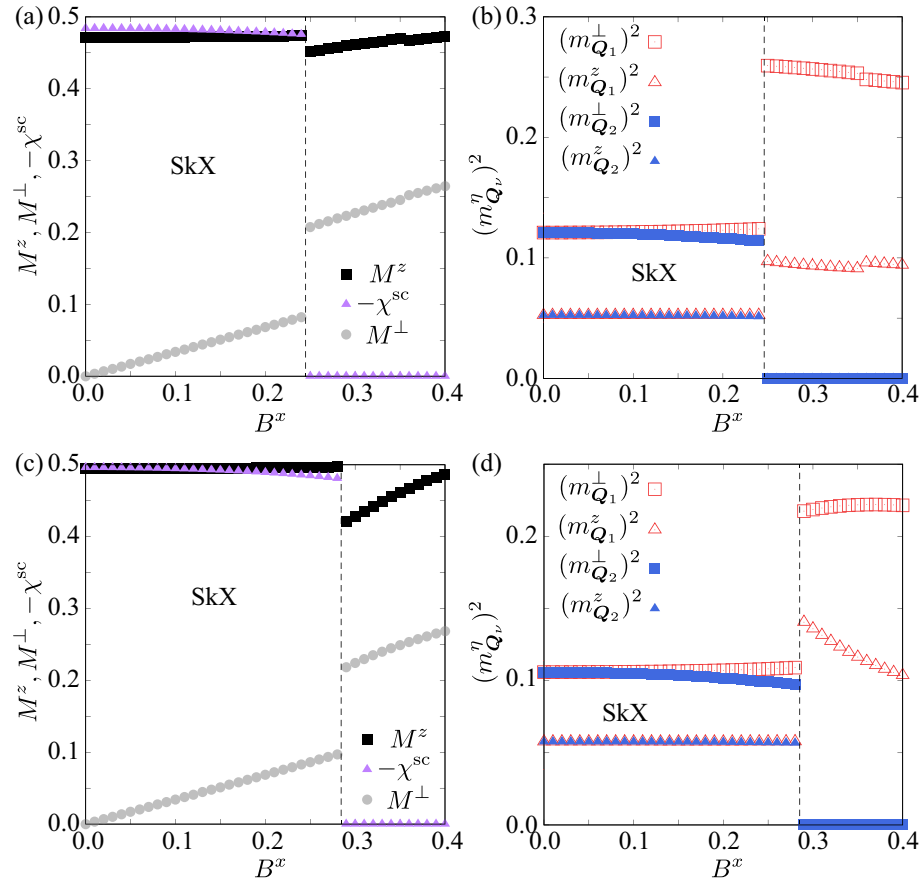


Figure 8. B^x dependence of (a,c) the in-plane magnetization, M^\perp , the out-of-plane magnetization, M^z , and the scalar spin chirality, χ^{sc} , and (b,d) the squared momentum-resolved magnetic moments $(m_{Q_\nu}^\eta)^2$ for $\eta = \pm, z$ and $\nu = 1, 2$ at (a,b) $I^z = 0.2$ and $B^z = 1.5$ and (c,d) $I^z = 0.4$ and $B^z = 1.7$. The vertical dashed lines represent the phase boundaries between the SkXs and other topologically trivial magnetic phases.

Meanwhile, the opposite stability tendency is found in the case of the easy-plane anisotropic interaction $I^z < 0$. As shown by the phase diagrams for $I^z = -0.2$ in Figure 5d and for $I^z = -0.4$ in Figure 5e, the SkX is more robust against B^z for smaller I^z , while it is more fragile against B^x for smaller I^z . The SkX shows the transition to the single-Q state at $B^x \simeq 0.14$ for $B^z = 1.2$, in the case of $I^z = -0.2$ in Figure 9a,b, and at $B^x \simeq 0.09$ for $B^z = 1.0$, in the case of $I^z = -0.4$ in Figure 9c,d. Such a stability feature is common to the SkX in centrosymmetric magnets; the SkX becomes robust against B^x when the easy-plane anisotropic interaction is weak [130–132].

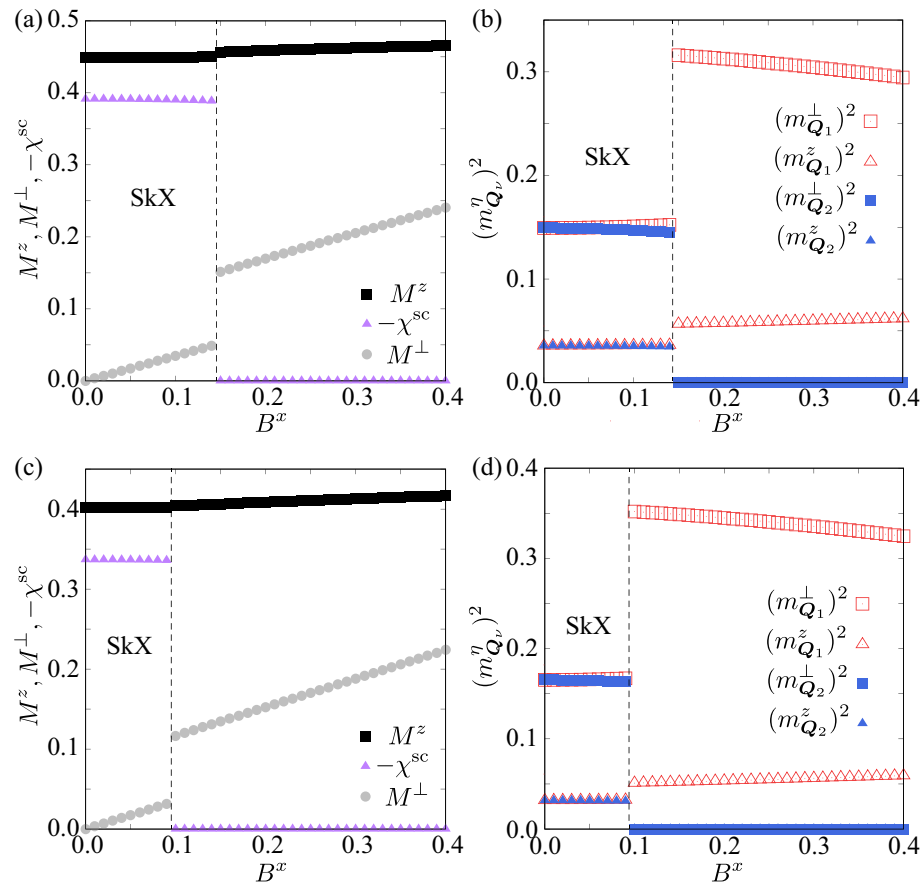


Figure 9. B^x dependence of (a,c) the in-plane magnetization, M^\perp , the out-of-plane magnetization, M^z , and the scalar spin chirality, χ^{sc} , and (b,d) the squared momentum-resolved magnetic moments $(m_{Q_\nu}^\eta)^2$ for $\eta = \perp, z$ and $\nu = 1, 2$ at (a,b) $I^z = -0.2$ and $B^z = 1.2$ and (c,d) $I^z = -0.4$ and $B^z = 1.0$. The vertical dashed lines represent the phase boundaries between the SkXs and other topologically trivial magnetic phases.

4. Conclusions

We have investigated the stability of the square SkX in noncentrosymmetric tetragonal magnets by focusing on the easy-plane and easy-axis anisotropic interactions. The systematic numerical analysis based on the simulated annealing for the spin model reveals the opposite stability tendency of the square SkX in the presence of the magnetic anisotropic interaction when the in-plane and out-of-plane magnetic fields are varied. We have shown that the SkX in the presence of the easy-plane anisotropic interaction is more robust than that in the presence of the easy-axis one when the out-of-plane magnetic field is changed. On the other hand, the opposite stability tendency is found when the magnetic field is tilted to the in-plane direction; the SkX under the easy-axis anisotropic interaction is more robust than that under the easy-plane one. Our results indicate that the degree of the easy-axis/easy-plane anisotropy does not affect the stability of the square SkX at the qualitative level, but affects the quantitative level. Since the present discussion can be applied to the

SkX induced by the DM interaction, a similar stability tendency is expected in the SkX in centrosymmetric magnets with the staggered-type DM interaction [133–135].

Funding: This research was supported by JSPS KAKENHI Grants Numbers JP21H01037, JP22H00101, JP22H01183, JP23H04869, JP23K03288, JP23K20827, and by JST CREST (JPMJCR23O4).

Institutional Review Board Statement: Not applicable.

Informed Consent Statement: Not applicable.

Data Availability Statement: The original contributions presented in the study are included in the article. Further inquiries can be directed to the corresponding author.

Conflicts of Interest: The author declares no conflicts of interest.

References

1. Aizu, K. Polarization, Pyroelectricity, and Ferroelectricity of Ionic Crystals. *Rev. Mod. Phys.* **1962**, *34*, 550–576. [[CrossRef](#)]
2. Dresselhaus, M.S.; Dresselhaus, G.; Jorio, A. *Group Theory: Application to the Physics of Condensed Matter*; Springer: Berlin/Heidelberg, Germany, 2008.
3. Frigeri, P.A.; Agterberg, D.F.; Sigrist, M. Spin susceptibility in superconductors without inversion symmetry. *N. J. Phys.* **2004**, *6*, 115. [[CrossRef](#)]
4. Palazzese, S.; Landaeta, J.; Subero, D.; Bauer, E.; Bonalde, I. Strong antisymmetric spin-orbit coupling and superconducting properties: The case of noncentrosymmetric LaPtSi. *J. Phys. Condens. Matter.* **2018**, *30*, 255603. [[CrossRef](#)] [[PubMed](#)]
5. Hayami, S.; Yanagi, Y.; Kusunose, H. Spontaneous antisymmetric spin splitting in noncollinear antiferromagnets without spin-orbit coupling. *Phys. Rev. B* **2020**, *101*, 220403(R). [[CrossRef](#)]
6. Rashba, E.I. Properties of semiconductors with an extremum loop. 1. Cyclotron and combinational resonance in a magnetic field perpendicular to the plane of the loop. *Sov. Phys. Solid State* **1960**, *2*, 1109–1122.
7. Ishizaka, K.; Bahramy, M.; Murakawa, H.; Sakano, M.; Shimojima, T.; Sonobe, T.; Koizumi, K.; Shin, S.; Miyahara, H.; Kimura, A.; et al. Giant Rashba-type spin splitting in bulk BiTeI. *Nat. Mater.* **2011**, *10*, 521–526. [[CrossRef](#)] [[PubMed](#)]
8. Bahramy, M.S.; Arita, R.; Nagaosa, N. Origin of giant bulk Rashba splitting: Application to BiTeI. *Phys. Rev. B* **2011**, *84*, 041202(R). [[CrossRef](#)]
9. Sunko, V.; Rosner, H.; Kushwaha, P.; Khim, S.; Mazzola, F.; Bawden, L.; Clark, O.; Riley, J.; Kasinathan, D.; Haverkort, M.; et al. Maximal Rashba-like spin splitting via kinetic-energy-coupled inversion-symmetry breaking. *Nature* **2017**, *549*, 492–496. [[CrossRef](#)]
10. Takashima, R.; Fujimoto, S. Supercurrent-induced skyrmion dynamics and tunable Weyl points in chiral magnet with superconductivity. *Phys. Rev. B* **2016**, *94*, 235117. [[CrossRef](#)]
11. Wang, B.Z.; Lu, Y.H.; Sun, W.; Chen, S.; Deng, Y.; Liu, X.J. Dirac-, Rashba-, and Weyl-type spin-orbit couplings: Toward experimental realization in ultracold atoms. *Phys. Rev. A* **2018**, *97*, 011605(R). [[CrossRef](#)]
12. Zhu, Z.Y.; Cheng, Y.C.; Schwingenschlögl, U. Giant spin-orbit-induced spin splitting in two-dimensional transition-metal dichalcogenide semiconductors. *Phys. Rev. B* **2011**, *84*, 153402. [[CrossRef](#)]
13. Wang, Q.H.; Kalantar-Zadeh, K.; Kis, A.; Coleman, J.N.; Strano, M.S. Electronics and optoelectronics of two-dimensional transition metal dichalcogenides. *Nat. Nanotechnol.* **2012**, *7*, 699. [[CrossRef](#)] [[PubMed](#)]
14. Ugeda, M.M.; Bradley, A.J.; Shi, S.F.; Felipe, H.; Zhang, Y.; Qiu, D.Y.; Ruan, W.; Mo, S.K.; Hussain, Z.; Shen, Z.X.; et al. Giant bandgap renormalization and excitonic effects in a monolayer transition metal dichalcogenide semiconductor. *Nat. Mater.* **2014**, *13*, 1091. [[CrossRef](#)] [[PubMed](#)]
15. Kormányos, A.; Zólyomi, V.; Drummond, N.D.; Burkard, G. Spin-Orbit Coupling, Quantum Dots, and Qubits in Monolayer Transition Metal Dichalcogenides. *Phys. Rev. X* **2014**, *4*, 011034. [[CrossRef](#)]
16. Hayami, S.; Kusunose, H.; Motome, Y. Spontaneous parity breaking in spin-orbital coupled systems. *Phys. Rev. B* **2014**, *90*, 081115. [[CrossRef](#)]
17. Murakami, S.; Nagaosa, N.; Zhang, S.C. Dissipationless quantum spin current at room temperature. *Science* **2003**, *301*, 1348–1351. [[CrossRef](#)]
18. Murakami, S.; Nagaosa, N.; Zhang, S.C. Spin-Hall Insulator. *Phys. Rev. Lett.* **2004**, *93*, 156804. [[CrossRef](#)]
19. Sinova, J.; Culcer, D.; Niu, Q.; Sinitsyn, N.A.; Jungwirth, T.; MacDonald, A.H. Universal Intrinsic Spin Hall Effect. *Phys. Rev. Lett.* **2004**, *92*, 126603. [[CrossRef](#)]
20. Fujimoto, S. Emergent Nodal Excitations due to Coexistence of Superconductivity and Antiferromagnetism: Cases with and without Inversion Symmetry. *J. Phys. Soc. Jpn.* **2006**, *75*, 083704. [[CrossRef](#)]
21. Fujimoto, S. Fermi liquid theory for heavy fermion superconductors without inversion symmetry: Magnetism and transport coefficients. *J. Phys. Soc. Jpn.* **2007**, *76*, 034712. [[CrossRef](#)]
22. Edelstein, V.M. Spin polarization of conduction electrons induced by electric current in two-dimensional asymmetric electron systems. *Solid State Commun.* **1990**, *73*, 233–235. [[CrossRef](#)]
23. Yip, S.K. Two-dimensional superconductivity with strong spin-orbit interaction. *Phys. Rev. B* **2002**, *65*, 144508. [[CrossRef](#)]

24. Fujimoto, S. Magnetoelectric effects in heavy-fermion superconductors without inversion symmetry. *Phys. Rev. B* **2005**, *72*, 024515. [[CrossRef](#)]
25. Yoda, T.; Yokoyama, T.; Murakami, S. Orbital Edelstein Effect as a Condensed-Matter Analog of Solenoids. *Nano Lett.* **2018**, *18*, 916–920. [[CrossRef](#)]
26. Massarelli, G.; Wu, B.; Paramekanti, A. Orbital Edelstein effect from density-wave order. *Phys. Rev. B* **2019**, *100*, 075136. [[CrossRef](#)]
27. Roy, A.; Cerasoli, F.T.; Jayaraj, A.; Tenzin, K.; Nardelli, M.B.; Śląwińska, J. Long-range current-induced spin accumulation in chiral crystals. *npj Comput. Mater.* **2022**, *8*, 243. [[CrossRef](#)]
28. Tenzin, K.; Roy, A.; Cerasoli, F.T.; Jayaraj, A.; Nardelli, M.B.; Śląwińska, J. Collinear Rashba-Edelstein effect in nonmagnetic chiral materials. *Phys. Rev. B* **2023**, *108*, 245203. [[CrossRef](#)]
29. Miyahara, S.; Furukawa, N. Nonreciprocal Directional Dichroism and Toroidal magnons in Helical Magnets. *J. Phys. Soc. Jpn.* **2012**, *81*, 023712. [[CrossRef](#)]
30. Miyahara, S.; Furukawa, N. Theory of magneto-optical effects in helical multiferroic materials via toroidal magnon excitation. *Phys. Rev. B* **2014**, *89*, 195145. [[CrossRef](#)]
31. Seki, S.; Okamura, Y.; Kondou, K.; Shibata, K.; Kubota, M.; Takagi, R.; Kagawa, F.; Kawasaki, M.; Tatara, G.; Otani, Y.; et al. Magnetochiral nonreciprocity of volume spin wave propagation in chiral-lattice ferromagnets. *Phys. Rev. B* **2016**, *93*, 235131. [[CrossRef](#)]
32. Giordano, A.; Verba, R.; Zivieri, R.; Laudani, A.; Puliafito, V.; Gubbiotti, G.; Tomasello, R.; Siracusano, G.; Azzerboni, B.; Carpentieri, M.; et al. Spin-Hall nano-oscillator with oblique magnetization and Dzyaloshinskii-Moriya interaction as generator of skyrmions and nonreciprocal spin-waves. *Sci. Rep.* **2016**, *6*, 36020. [[CrossRef](#)] [[PubMed](#)]
33. Tokura, Y.; Nagaosa, N. Nonreciprocal responses from non-centrosymmetric quantum materials. *Nat. Commun.* **2018**, *9*, 3740. [[CrossRef](#)] [[PubMed](#)]
34. Yokouchi, T.; Hoshino, S.; Kanazawa, N.; Kikkawa, A.; Morikawa, D.; Shibata, K.; Arima, T.H.; Taguchi, Y.; Kagawa, F.; Nagaosa, N.; et al. Current-induced dynamics of skyrmion strings. *Sci. Adv.* **2018**, *4*, eaat1115. [[CrossRef](#)] [[PubMed](#)]
35. Hoshino, S.; Nagaosa, N. Theory of the magnetic skyrmion glass. *Phys. Rev. B* **2018**, *97*, 024413. [[CrossRef](#)]
36. Bar'yakhtar, V.G.; Danilevich, A.G.; Krivoruchko, V.N. Magnetochiral nonreciprocity of spin wave damping in long-period structures. *Phys. Rev. B* **2019**, *99*, 104407. [[CrossRef](#)]
37. dos Santos, F.J.; dos Santos Dias, M.; Lounis, S. Nonreciprocity of spin waves in noncollinear magnets due to the Dzyaloshinskii-Moriya interaction. *Phys. Rev. B* **2020**, *102*, 104401. [[CrossRef](#)]
38. Seki, S.; Garst, M.; Waizner, J.; Takagi, R.; Khanh, N.; Okamura, Y.; Kondou, K.; Kagawa, F.; Otani, Y.; Tokura, Y. Propagation dynamics of spin excitations along skyrmion strings. *Nat. Commun.* **2020**, *11*, 256. [[CrossRef](#)]
39. Hayami, S.; Yatsushiro, M. Nonlinear nonreciprocal transport in antiferromagnets free from spin-orbit coupling. *Phys. Rev. B* **2022**, *106*, 014420. [[CrossRef](#)]
40. Katsura, H.; Nagaosa, N.; Balatsky, A.V. Spin Current and Magnetoelectric Effect in Noncollinear Magnets. *Phys. Rev. Lett.* **2005**, *95*, 057205. [[CrossRef](#)]
41. Mostovoy, M. Ferroelectricity in Spiral Magnets. *Phys. Rev. Lett.* **2006**, *96*, 067601. [[CrossRef](#)]
42. Cheong, S.W.; Mostovoy, M. Multiferroics: A magnetic twist for ferroelectricity. *Nat. Mater.* **2007**, *6*, 13–20. [[CrossRef](#)] [[PubMed](#)]
43. Bulaevskii, L.N.; Batista, C.D.; Mostovoy, M.V.; Khomskii, D.I. Electronic orbital currents and polarization in Mott insulators. *Phys. Rev. B* **2008**, *78*, 024402. [[CrossRef](#)]
44. Seki, S.; Yu, X.Z.; Ishiwata, S.; Tokura, Y. Observation of skyrmions in a multiferroic material. *Science* **2012**, *336*, 198–201. [[CrossRef](#)] [[PubMed](#)]
45. White, J.S.; Levatić, I.; Omrani, A.; Egetenmeyer, N.; Prša, K.; Živković, I.; Gavilano, J.L.; Kohlbrecher, J.; Bartkowiak, M.; Berger, H.; et al. Electric field control of the skyrmion lattice in Cu₂OSeO₃. *J. Phys. Condens. Matter.* **2012**, *24*, 432201. [[CrossRef](#)] [[PubMed](#)]
46. Tokura, Y.; Seki, S.; Nagaosa, N. Multiferroics of spin origin. *Rep. Prog. Phys.* **2014**, *77*, 076501. [[CrossRef](#)] [[PubMed](#)]
47. Mochizuki, M.; Seki, S. Dynamical magnetoelectric phenomena of multiferroic skyrmions. *J. Phys. Condens. Matter* **2015**, *27*, 503001. [[CrossRef](#)] [[PubMed](#)]
48. Hayami, S.; Kusunose, H.; Motome, Y. Spontaneous Multipole Ordering by Local Parity Mixing. *J. Phys. Soc. Jpn.* **2015**, *84*, 064717. [[CrossRef](#)]
49. Göbel, B.; Mook, A.; Henk, J.; Mertig, I. Magnetoelectric effect and orbital magnetization in skyrmion crystals: Detection and characterization of skyrmions. *Phys. Rev. B* **2019**, *99*, 060406. [[CrossRef](#)]
50. Kurumaji, T. Spiral spin structures and skyrmions in multiferroics. *Phys. Sci. Rev.* **2020**, *5*, 20190016. [[CrossRef](#)]
51. Dzyaloshinsky, I. A thermodynamic theory of “weak” ferromagnetism of antiferromagnetics. *J. Phys. Chem. Solids* **1958**, *4*, 241–255. [[CrossRef](#)]
52. Moriya, T. Anisotropic superexchange interaction and weak ferromagnetism. *Phys. Rev.* **1960**, *120*, 91. [[CrossRef](#)]
53. Rößler, U.K.; Bogdanov, A.N.; Pfleiderer, C. Spontaneous skyrmion ground states in magnetic metals. *Nature* **2006**, *442*, 797–801. [[CrossRef](#)] [[PubMed](#)]
54. Mühlbauer, S.; Binz, B.; Jonietz, F.; Pfleiderer, C.; Rosch, A.; Neubauer, A.; Georgii, R.; Böni, P. Skyrmion lattice in a chiral magnet. *Science* **2009**, *323*, 915–919. [[CrossRef](#)] [[PubMed](#)]

55. Yu, X.Z.; Onose, Y.; Kanazawa, N.; Park, J.H.; Han, J.H.; Matsui, Y.; Nagaosa, N.; Tokura, Y. Real-space observation of a two-dimensional skyrmion crystal. *Nature* **2010**, *465*, 901–904. [[CrossRef](#)]
56. Yi, S.D.; Onoda, S.; Nagaosa, N.; Han, J.H. Skyrmions and anomalous Hall effect in a Dzyaloshinskii-Moriya spiral magnet. *Phys. Rev. B* **2009**, *80*, 054416. [[CrossRef](#)]
57. Binz, B.; Vishwanath, A.; Aji, V. Theory of the Helical Spin Crystal: A Candidate for the Partially Ordered State of MnSi. *Phys. Rev. Lett.* **2006**, *96*, 207202. [[CrossRef](#)]
58. Binz, B.; Vishwanath, A. Theory of helical spin crystals: Phases, textures, and properties. *Phys. Rev. B* **2006**, *74*, 214408. [[CrossRef](#)]
59. Nagaosa, N.; Tokura, Y. Topological properties and dynamics of magnetic skyrmions. *Nat. Nanotechnol.* **2013**, *8*, 899–911. [[CrossRef](#)]
60. Tokura, Y.; Kanazawa, N. Magnetic Skyrmion Materials. *Chem. Rev.* **2021**, *121*, 2857. [[CrossRef](#)]
61. Balasubramanian, B.; Manchanda, P.; Pahari, R.; Chen, Z.; Zhang, W.; Valloppilly, S.R.; Li, X.; Sarella, A.; Yue, L.; Ullah, A.; et al. Chiral Magnetism and High-Temperature Skyrmions in B20-Ordered Co-Si. *Phys. Rev. Lett.* **2020**, *124*, 057201. [[CrossRef](#)]
62. Bogdanov, A.N.; Yablonskii, D.A. Thermodynamically stable “vortices” in magnetically ordered crystals: The mixed state of magnets. *Sov. Phys. JETP* **1989**, *68*, 101.
63. Bogdanov, A.; Hubert, A. Thermodynamically stable magnetic vortex states in magnetic crystals. *J. Magn. Magn. Mater.* **1994**, *138*, 255–269. [[CrossRef](#)]
64. Ohgushi, K.; Murakami, S.; Nagaosa, N. Spin anisotropy and quantum Hall effect in the *kagomé* lattice: Chiral spin state based on a ferromagnet. *Phys. Rev. B* **2000**, *62*, R6065–R6068. [[CrossRef](#)]
65. Taguchi, Y.; Oohara, Y.; Yoshizawa, H.; Nagaosa, N.; Tokura, Y. Spin chirality, Berry phase, and anomalous Hall effect in a frustrated ferromagnet. *Science* **2001**, *291*, 2573–2576. [[CrossRef](#)] [[PubMed](#)]
66. Tataro, G.; Kawamura, H. Chirality-driven anomalous Hall effect in weak coupling regime. *J. Phys. Soc. Jpn.* **2002**, *71*, 2613–2616. [[CrossRef](#)]
67. Neubauer, A.; Pfleiderer, C.; Binz, B.; Rosch, A.; Ritz, R.; Niklowitz, P.G.; Böni, P. Topological Hall Effect in the A Phase of MnSi. *Phys. Rev. Lett.* **2009**, *102*, 186602. [[CrossRef](#)] [[PubMed](#)]
68. Shiomi, Y.; Kanazawa, N.; Shibata, K.; Onose, Y.; Tokura, Y. Topological Nernst effect in a three-dimensional skyrmion-lattice phase. *Phys. Rev. B* **2013**, *88*, 064409. [[CrossRef](#)]
69. Hamamoto, K.; Ezawa, M.; Nagaosa, N. Quantized topological Hall effect in skyrmion crystal. *Phys. Rev. B* **2015**, *92*, 115417. [[CrossRef](#)]
70. Nakazawa, K.; Bibes, M.; Kohno, H. Topological Hall effect from strong to weak coupling. *J. Phys. Soc. Jpn.* **2018**, *87*, 033705. [[CrossRef](#)]
71. Zadorozhnyi, A.; Dahnovsky, Y. Topological Hall effect in three-dimensional centrosymmetric magnetic skyrmion crystals. *Phys. Rev. B* **2023**, *107*, 054436. [[CrossRef](#)]
72. Zhang, C.; Liu, C.; Zhang, J.; Yuan, Y.; Wen, Y.; Li, Y.; Zheng, D.; Zhang, Q.; Hou, Z.; Yin, G.; et al. Room-Temperature Magnetic Skyrmions and Large Topological Hall Effect in Chromium Telluride Engineered by Self-Intercalation. *Adv. Mater.* **2023**, *35*, 2205967. [[CrossRef](#)] [[PubMed](#)]
73. Jonietz, F.; Mühlbauer, S.; Pfleiderer, C.; Neubauer, A.; Münzer, W.; Bauer, A.; Adams, T.; Georgii, R.; Böni, P.; Duine, R.A.; et al. Spin Transfer Torques in MnSi at Ultralow Current Densities. *Science* **2010**, *330*, 1648. [[CrossRef](#)] [[PubMed](#)]
74. Yu, X.Z.; Kanazawa, N.; Zhang, W.; Nagai, T.; Hara, T.; Kimoto, K.; Matsui, Y.; Onose, Y.; Tokura, Y. Skyrmion flow near room temperature in an ultralow current density. *Nat. Commun.* **2012**, *3*, 988. [[CrossRef](#)] [[PubMed](#)]
75. Jiang, W.; Zhang, X.; Yu, G.; Zhang, W.; Wang, X.; Benjamin Jungfleisch, M.; Pearson, J.E.; Cheng, X.; Heinonen, O.; Wang, K.L.; et al. Direct observation of the skyrmion Hall effect. *Nat. Phys.* **2017**, *13*, 162–169. [[CrossRef](#)]
76. Yu, X.; Morikawa, D.; Nakajima, K.; Shibata, K.; Kanazawa, N.; Arima, T.h.; Nagaosa, N.; Tokura, Y. Motion tracking of 80-nm-size skyrmions upon directional current injections. *Sci. Adv.* **2020**, *6*, eaaz9744. [[CrossRef](#)]
77. Pham, V.T.; Sisodia, N.; Di Manici, I.; Urrestarazu-Larrañaga, J.; Bairagi, K.; Pelloux-Prayer, J.; Guedas, R.; Buda-Prejbeanu, L.D.; Auffret, S.; Locatelli, A.; et al. Fast current-induced skyrmion motion in synthetic antiferromagnets. *Science* **2024**, *384*, 307–312. [[CrossRef](#)]
78. Song, D.; Wang, W.; Zhang, S.; Liu, Y.; Wang, N.; Zheng, F.; Tian, M.; Dunin-Borkowski, R.E.; Zang, J.; Du, H. Steady motion of 80-nm-size skyrmions in a 100-nm-wide track. *Nat. Commun.* **2024**, *15*, 5614. [[CrossRef](#)]
79. Ji, Y.; Yang, S.; Ahn, H.B.; Moon, K.W.; Ju, T.S.; Im, M.Y.; Han, H.S.; Lee, J.; Park, S.y.; Lee, C.; et al. Direct Observation of Room-Temperature Magnetic Skyrmion Motion Driven by Ultra-Low Current Density in Van Der Waals Ferromagnets. *Adv. Mater.* **2024**, *36*, 2312013. [[CrossRef](#)]
80. Birch, M.T.; Belopolski, I.; Fujiishi, Y.; Kawamura, M.; Kikkawa, A.; Taguchi, Y.; Hirschberger, M.; Nagaosa, N.; Tokura, Y. Dynamic transition and Galilean relativity of current-driven skyrmions. *Nature* **2024**, *633*, 554–559. [[CrossRef](#)]
81. Jiang, W.; Upadhyaya, P.; Zhang, W.; Yu, G.; Jungfleisch, M.B.; Fradin, F.Y.; Pearson, J.E.; Tserkovnyak, Y.; Wang, K.L.; Heinonen, O.; et al. Blowing magnetic skyrmion bubbles. *Science* **2015**, *349*, 283–286. [[CrossRef](#)]
82. Büttner, F.; Lemesh, I.; Schneider, M.; Pfau, B.; Günther, C.M.; Hessing, P.; Geilhufe, J.; Caretta, L.; Engel, D.; Krüger, B.; et al. Field-free deterministic ultrafast creation of magnetic skyrmions by spin-orbit torques. *Nat. Nanotechnol.* **2017**, *12*, 1040–1044. [[CrossRef](#)] [[PubMed](#)]

83. Hrabec, A.; Sampaio, J.; Belmeguenai, M.; Gross, I.; Weil, R.; Chérif, S.M.; Stashkevich, A.; Jacques, V.; Thiaville, A.; Rohart, S. Current-induced skyrmion generation and dynamics in symmetric bilayers. *Nat. Commun.* **2017**, *8*, 15765. [[CrossRef](#)] [[PubMed](#)]
84. Ahrens, V.; Kiesselbach, C.; Gnoli, L.; Giuliano, D.; Mendisch, S.; Kiechle, M.; Riente, F.; Becherer, M. Skyrmions Under Control—FIB Irradiation as a Versatile Tool for Skyrmion Circuits. *Adv. Mater.* **2023**, *35*, 2207321. [[CrossRef](#)] [[PubMed](#)]
85. de Jong, M.C.H.; Smit, B.H.M.; Meijer, M.J.; Lucassen, J.; Swagten, H.J.M.; Koopmans, B.; Lavrijsen, R. Controlling magnetic skyrmion nucleation with Ga^+ ion irradiation. *Phys. Rev. B* **2023**, *107*, 094429. [[CrossRef](#)]
86. Li, S.; Wang, X.; Rasing, T. Magnetic skyrmions: Basic properties and potential applications. *Interdiscip. Mater.* **2023**, *2*, 260–289. [[CrossRef](#)]
87. Wang, X.; Li, M.; Li, B.; Li, Y.; Li, Y.; Zheng, F.; Liu, L. Efficient generation and deterministic annihilation of a single skyrmion via pure localized heating. *J. Appl. Phys.* **2024**, *135*, 143902. [[CrossRef](#)]
88. Butenko, A.B.; Leonov, A.A.; Rößler, U.K.; Bogdanov, A.N. Stabilization of skyrmion textures by uniaxial distortions in noncentrosymmetric cubic helimagnets. *Phys. Rev. B* **2010**, *82*, 052403. [[CrossRef](#)]
89. Wilson, M.N.; Butenko, A.B.; Bogdanov, A.N.; Monchesky, T.L. Chiral skyrmions in cubic helimagnet films: The role of uniaxial anisotropy. *Phys. Rev. B* **2014**, *89*, 094411. [[CrossRef](#)]
90. Lin, S.Z.; Saxena, A.; Batista, C.D. Skyrmion fractionalization and merons in chiral magnets with easy-plane anisotropy. *Phys. Rev. B* **2015**, *91*, 224407. [[CrossRef](#)]
91. Leonov, A.O.; Monchesky, T.L.; Romming, N.; Kubetzka, A.; Bogdanov, A.N.; Wiesendanger, R. The properties of isolated chiral skyrmions in thin magnetic films. *N. J. Phys.* **2016**, *18*, 065003. [[CrossRef](#)]
92. Leonov, A.O.; Kézsmárki, I. Asymmetric isolated skyrmions in polar magnets with easy-plane anisotropy. *Phys. Rev. B* **2017**, *96*, 014423. [[CrossRef](#)]
93. Hayami, S.; Motome, Y. Néel- and Bloch-Type Magnetic Vortices in Rashba Metals. *Phys. Rev. Lett.* **2018**, *121*, 137202. [[CrossRef](#)]
94. Hayami, S. Rectangular and square skyrmion crystals on a centrosymmetric square lattice with easy-axis anisotropy. *Phys. Rev. B* **2022**, *105*, 174437. [[CrossRef](#)]
95. Tokunaga, Y.; Yu, X.; White, J.; Rønnow, H.M.; Morikawa, D.; Taguchi, Y.; Tokura, Y. A new class of chiral materials hosting magnetic skyrmions beyond room temperature. *Nat. Commun.* **2015**, *6*, 7638. [[CrossRef](#)] [[PubMed](#)]
96. Karube, K.; White, J.; Reynolds, N.; Gavilano, J.; Oike, H.; Kikkawa, A.; Kagawa, F.; Tokunaga, Y.; Rønnow, H.M.; Tokura, Y.; et al. Robust metastable skyrmions and their triangular–square lattice structural transition in a high-temperature chiral magnet. *Nat. Mater.* **2016**, *15*, 1237. [[CrossRef](#)] [[PubMed](#)]
97. Karube, K.; White, J.S.; Morikawa, D.; Dewhurst, C.D.; Cubitt, R.; Kikkawa, A.; Yu, X.; Tokunaga, Y.; Arima, T.h.; Rønnow, H.M.; et al. Disordered skyrmion phase stabilized by magnetic frustration in a chiral magnet. *Sci. Adv.* **2018**, *4*, eaar7043. [[CrossRef](#)]
98. Karube, K.; White, J.S.; Ukleev, V.; Dewhurst, C.D.; Cubitt, R.; Kikkawa, A.; Tokunaga, Y.; Rønnow, H.M.; Tokura, Y.; Taguchi, Y. Metastable skyrmion lattices governed by magnetic disorder and anisotropy in β -Mn-type chiral magnets. *Phys. Rev. B* **2020**, *102*, 064408. [[CrossRef](#)]
99. Henderson, M.E.; Bleuel, M.; Beare, J.; Cory, D.G.; Heacock, B.; Huber, M.G.; Luke, G.M.; Pula, M.; Sarenac, D.; Sharma, S.; et al. Skyrmion alignment and pinning effects in the disordered multiphase skyrmion material $\text{Co}_8\text{Zn}_8\text{Mn}_4$. *Phys. Rev. B* **2022**, *106*, 094435. [[CrossRef](#)]
100. Chacon, A.; Heinen, L.; Halder, M.; Bauer, A.; Simeth, W.; Mühlbauer, S.; Berger, H.; Garst, M.; Rosch, A.; Pfleiderer, C. Observation of two independent skyrmion phases in a chiral magnetic material. *Nat. Phys.* **2018**, *14*, 936–941. [[CrossRef](#)]
101. Takagi, R.; Yamasaki, Y.; Yokouchi, T.; Ukleev, V.; Yokoyama, Y.; Nakao, H.; Arima, T.; Tokura, Y.; Seki, S. Particle-size dependent structural transformation of skyrmion lattice. *Nat. Commun.* **2020**, *11*, 5685. [[CrossRef](#)]
102. Khanh, N.D.; Nakajima, T.; Yu, X.; Gao, S.; Shibata, K.; Hirschberger, M.; Yamasaki, Y.; Sagayama, H.; Nakao, H.; Peng, L.; et al. Nanometric square skyrmion lattice in a centrosymmetric tetragonal magnet. *Nat. Nanotechnol.* **2020**, *15*, 444. [[CrossRef](#)] [[PubMed](#)]
103. Khanh, N.D.; Nakajima, T.; Hayami, S.; Gao, S.; Yamasaki, Y.; Sagayama, H.; Nakao, H.; Takagi, R.; Motome, Y.; Tokura, Y.; et al. Zoology of Multiple-Q Spin Textures in a Centrosymmetric Tetragonal Magnet with Itinerant Electrons. *Adv. Sci.* **2022**, *9*, 2105452. [[CrossRef](#)] [[PubMed](#)]
104. Matsuyama, N.; Nomura, T.; Imajo, S.; Nomoto, T.; Arita, R.; Sudo, K.; Kimata, M.; Khanh, N.D.; Takagi, R.; Tokura, Y.; et al. Quantum oscillations in the centrosymmetric skyrmion-hosting magnet GdRu_2Si_2 . *Phys. Rev. B* **2023**, *107*, 104421. [[CrossRef](#)]
105. Wood, G.D.A.; Khalyavin, D.D.; Mayoh, D.A.; Bouaziz, J.; Hall, A.E.; Holt, S.J.R.; Orlandi, F.; Manuel, P.; Blügel, S.; Staunton, J.B.; et al. Double-Q ground state with topological charge stripes in the centrosymmetric skyrmion candidate GdRu_2Si_2 . *Phys. Rev. B* **2023**, *107*, L180402. [[CrossRef](#)]
106. Eremeev, S.; Glazkova, D.; Poelchen, G.; Kraiker, A.; Ali, K.; Tarasov, A.V.; Schulz, S.; Kliemt, K.; Chulkov, E.V.; Stolyarov, V.; et al. Insight into the electronic structure of the centrosymmetric skyrmion magnet GdRu_2Si_2 . *Nanoscale Adv.* **2023**, *5*, 6678–6687. [[CrossRef](#)] [[PubMed](#)]
107. Yoshimochi, H.; Takagi, R.; Ju, J.; Khanh, N.; Saito, H.; Sagayama, H.; Nakao, H.; Itoh, S.; Tokura, Y.; Arima, T.; et al. Multistep topological transitions among meron and skyrmion crystals in a centrosymmetric magnet. *Nat. Phys.* **2024**, *20*, 1001. [[CrossRef](#)]
108. Hayami, S.; Yambe, R. Stabilization mechanisms of magnetic skyrmion crystal and multiple-Q states based on momentum-resolved spin interactions. *Mater. Today Quantum* **2024**, *3*, 100010. [[CrossRef](#)]
109. Hayami, S.; Motome, Y. Topological spin crystals by itinerant frustration. *J. Phys.: Condens. Matter* **2021**, *33*, 443001. [[CrossRef](#)]

110. Ruderman, M.A.; Kittel, C. Indirect Exchange Coupling of Nuclear Magnetic Moments by Conduction Electrons. *Phys. Rev.* **1954**, *96*, 99–102. [[CrossRef](#)]
111. Kasuya, T. A Theory of Metallic Ferro- and Antiferromagnetism on Zener’s Model. *Prog. Theor. Phys.* **1956**, *16*, 45–57. [[CrossRef](#)]
112. Yosida, K. Magnetic Properties of Cu-Mn Alloys. *Phys. Rev.* **1957**, *106*, 893–898. [[CrossRef](#)]
113. Ullah, A.; Balamurugan, B.; Zhang, W.; Valloppilly, S.; Li, X.Z.; Pahari, R.; Yue, L.P.; Sokolov, A.; Sellmyer, D.J.; Skomski, R. Crystal structure and Dzyaloshinski-Moriya micromagnetics. *IEEE Trans. Magn.* **2019**, *55*, 1–5. [[CrossRef](#)]
114. Yambe, R.; Hayami, S. Effective spin model in momentum space: Toward a systematic understanding of multiple-Q instability by momentum-resolved anisotropic exchange interactions. *Phys. Rev. B* **2022**, *106*, 174437. [[CrossRef](#)]
115. Ullah, A.; Balasubramanian, B.; Tiwari, B.; Giri, B.; Sellmyer, D.J.; Skomski, R.; Xu, X. Topological spin textures and topological Hall effect in centrosymmetric magnetic nanoparticles. *Phys. Rev. B* **2023**, *108*, 184432. [[CrossRef](#)]
116. Berg, B.; L’uscher, M. Definition and statistical distributions of a topological number in the lattice O(3) σ -model. *Nucl. Phys. B* **1981**, *190*, 412–424. [[CrossRef](#)]
117. Hayami, S.; Yambe, R. Locking of skyrmion cores on a centrosymmetric discrete lattice: Onsite versus offsite. *Phys. Rev. Res.* **2021**, *3*, 043158. [[CrossRef](#)]
118. Hayami, S.; Motome, Y. Effect of magnetic anisotropy on skyrmions with a high topological number in itinerant magnets. *Phys. Rev. B* **2019**, *99*, 094420. [[CrossRef](#)]
119. Hayami, S. Multiple-Q magnetism by anisotropic bilinear-biquadratic interactions in momentum space. *J. Magn. Magn. Mater.* **2020**, *513*, 167181. [[CrossRef](#)]
120. Kakihana, M.; Aoki, D.; Nakamura, A.; Honda, F.; Nakashima, M.; Amako, Y.; Nakamura, S.; Sakakibara, T.; Hedo, M.; Nakama, T.; et al. Giant Hall resistivity and magnetoresistance in cubic chiral antiferromagnet EuPtSi. *J. Phys. Soc. Jpn.* **2018**, *87*, 023701. [[CrossRef](#)]
121. Kaneko, K.; Frontzek, M.D.; Matsuda, M.; Nakao, A.; Munakata, K.; Ohhara, T.; Kakihana, M.; Haga, Y.; Hedo, M.; Nakama, T.; et al. Unique Helical Magnetic Order and Field-Induced Phase in Trillium Lattice Antiferromagnet EuPtSi. *J. Phys. Soc. Jpn.* **2019**, *88*, 013702. [[CrossRef](#)]
122. Tabata, C.; Matsumura, T.; Nakao, H.; Michimura, S.; Kakihana, M.; Inami, T.; Kaneko, K.; Hedo, M.; Nakama, T.; Ōnuki, Y. Magnetic Field Induced Triple- q Magnetic Order in Trillium Lattice Antiferromagnet EuPtSi Studied by Resonant X-ray Scattering. *J. Phys. Soc. Jpn.* **2019**, *88*, 093704. [[CrossRef](#)]
123. Kakihana, M.; Aoki, D.; Nakamura, A.; Honda, F.; Nakashima, M.; Amako, Y.; Takeuchi, T.; Harima, H.; Hedo, M.; Nakama, T.; et al. Unique Magnetic Phases in the Skyrmion Lattice and Fermi Surface Properties in Cubic Chiral Antiferromagnet EuPtSi. *J. Phys. Soc. Jpn.* **2019**, *88*, 094705. [[CrossRef](#)]
124. Mishra, A.K.; Ganesan, V. A-phase, field-induced tricritical point, and universal magnetocaloric scaling in EuPtSi. *Phys. Rev. B* **2019**, *100*, 125113. [[CrossRef](#)]
125. Takeuchi, T.; Kakihana, M.; Hedo, M.; Nakama, T.; Ōnuki, Y. Magnetic field versus temperature phase diagram for $H \parallel [001]$ in the trillium lattice antiferromagnet EuPtSi. *J. Phys. Soc. Jpn.* **2019**, *88*, 053703. [[CrossRef](#)]
126. Matsumura, T.; Tabata, C.; Kaneko, K.; Nakao, H.; Kakihana, M.; Hedo, M.; Nakama, T.; Ōnuki, Y. Single helicity of the triple- q triangular skyrmion lattice state in the cubic chiral helimagnet EuPtSi. *Phys. Rev. B* **2024**, *109*, 174437. [[CrossRef](#)]
127. Takeuchi, T.; Kakihana, M.; Hedo, M.; Nakama, T.; Ōnuki, Y. Angle Dependence of the Magnetic Phase Diagram in Cubic Chiral Antiferromagnet EuPtSi. *J. Phys. Soc. Jpn.* **2020**, *89*, 093703. [[CrossRef](#)]
128. Hayami, S.; Yambe, R. Field-Direction Sensitive Skyrmion Crystals in Cubic Chiral Systems: Implication to 4f-Electron Compound EuPtSi. *J. Phys. Soc. Jpn.* **2021**, *90*, 073705. [[CrossRef](#)]
129. Sakakibara, T.; Nakamura, S.; Kittaka, S.; Kakihana, M.; Hedo, M.; Nakama, T.; Onuki, Y. Magnetic Phase Transitions of the 4f Skyrmion Compound EuPtSi Studied by Magnetization Measurements. *J. Phys. Soc. Jpn.* **2021**, *90*, 064701. [[CrossRef](#)]
130. Hayami, S. In-plane magnetic field-induced skyrmion crystal in frustrated magnets with easy-plane anisotropy. *Phys. Rev. B* **2021**, *103*, 224418. [[CrossRef](#)]
131. Hayami, S.; Motome, Y. Noncoplanar multiple-Q spin textures by itinerant frustration: Effects of single-ion anisotropy and bond-dependent anisotropy. *Phys. Rev. B* **2021**, *103*, 054422. [[CrossRef](#)]
132. Hirschberger, M.; Hayami, S.; Tokura, Y. Nanometric skyrmion lattice from anisotropic exchange interactions in a centrosymmetric host. *New J. Phys.* **2021**, *23*, 023039. [[CrossRef](#)]
133. Hayami, S. Skyrmion crystal and spiral phases in centrosymmetric bilayer magnets with staggered Dzyaloshinskii-Moriya interaction. *Phys. Rev. B* **2022**, *105*, 014408. [[CrossRef](#)]
134. Hayami, S. Multifarious skyrmion phases on a trilayer triangular lattice. *Phys. Rev. B* **2022**, *105*, 184426. [[CrossRef](#)]
135. Lin, S.Z. Skyrmion lattice in centrosymmetric magnets with local Dzyaloshinsky-Moriya interaction. *Mater. Today Quantum* **2024**, *2*, 100006. [[CrossRef](#)]

Disclaimer/Publisher’s Note: The statements, opinions and data contained in all publications are solely those of the individual author(s) and contributor(s) and not of MDPI and/or the editor(s). MDPI and/or the editor(s) disclaim responsibility for any injury to people or property resulting from any ideas, methods, instructions or products referred to in the content.